Improved Computation of Sum Frequency Generation Spectrum of the Surface of Water

Akihiro Morita*,†

Department of Computational Molecular Science, Institute for Molecular Science, Myodaiji, Okazaki 444-8585, Japan, and Graduate University for Advanced Studies, Myodaiji, Okazaki 444-8585, Japan

Received: May 9, 2005

The infrared-visible sum frequency generation (SFG) spectrum of the surface of water was calculated with significantly improved accuracy via the time-dependent formalism we have recently proposed. The revisions include molecular modeling of the OH stretching region, sampling statistics, and a treatment of boundary conditions. The calculated spectra show good agreement with recent experiments, allowing a detailed comparison and analysis.

1. Introduction

The infrared-visible sum frequency generation (SFG) technique is widely used as an interface vibrational spectroscopy.[1] This technique, based on second-order nonlinear processes, is intrinsically specific to interfaces when the bulk phases possess inversion symmetry. The surface sensitivity of this technique makes it particularly powerful for investigating interfaces in atmospheric conditions or for liquid interfaces (gas−liquid, liquid−liquid, solid−liquid); few other experimental probes have an equivalent surface sensitivity.[2−5]

Although vibrational SFG spectra include rich microscopic information about surface species, structure, orientation, density, etc., it is often not straightforward to exploit this information from the experimental spectra alone. Quantitative interpretation of the spectra is complicated by interference among the resonant amplitudes of vibrational modes and the nonresonant amplitude. These amplitudes are governed by both the number density of the surface species and their orientational distribution at the surface. Decomposition of an observed signal into these two factors is challenging in general. Therefore, theoretical analysis of SFG spectra is required to assist experimental analysis and interpretation.[6−9]

A key aspect of theoretical analysis is describing the vibrational contributions to the nonlinear susceptibility. We have proposed and developed two theoretical methods to compute SFG spectra by a combination of ab initio molecular modeling and molecular dynamics (MD) simulation. One method employs the energy representation of the frequency-dependent nonlinear susceptibility[6] and the other employs the time correlation function representation.[8] These two methods apply nonempirical computation of SFG spectra from a molecular model and have proven to be successful in reproducing the experimental SFG spectrum of the surface of water. In particular, the latter method is more suitable for making empirical parametrization unnecessary in deriving SFG spectra.[8] It should be noted that the latter method incorporates the motional effect on the resonant nonlinear susceptibility[10] and, accordingly, provides more rigorous and unambiguous analysis of SFG spectra within the electric dipole treatment, at the expense of a heavier computational cost. We also note that extending this method beyond the electric dipole approximation is under way.[11]

This paper adopts the time correlation function representation and presents revised and improved calculations of the SFG spectrum of the surface of water. Although this method can be quite accurate within the dipole approximation, its actual implementation is not straightforward and involves choosing the appropriate molecular modeling, statistical sampling of the surface structure, and boundaries of the molecular dynamics simulation.

2. Theory

The theory and computational method of SFG spectroscopy are described in detail elsewhere,[8] and hence, this section briefly summarizes the procedure with the quantum correction effects considered.

The focus of the present computation is the surface nonlinear dipolar susceptibility, $\chi(\omega_{SFG},\omega_{vis},\omega_{IR})$, defined as[12]

$$P(\omega_{SFG}) = \chi(\omega_{SFG},\omega_{vis},\omega_{IR})\, E(\omega_{vis})\, E(\omega_{IR}) \qquad (1)$$

where $P(\omega_{SFG})$ is the induced electric dipole polarization of the sum frequency $\omega_{SFG} = \omega_{vis} + \omega_{IR}$ at the surface and $E(\omega_{vis})$ and $E(\omega_{IR})$ are the external (vacuum) electric fields at visible and IR frequencies, respectively. The output intensity of the sum frequency $I(\omega_{SFG})$ is, thus, given as[12]

$$I(\omega_{SFG}) \sim \omega_{SFG}{}^2 |F_{SFG}\chi(\omega_{SFG},\omega_{vis},\omega_{IR})|^2 I(\omega_{vis})\, I(\omega_{IR}) \qquad (2)$$

where F_{SFG} is the nonlinear Fresnel coefficient for the output SFG field and $I(\omega_{vis})$ and $I(\omega_{IR})$ are the incident visible and IR intensities. The effects of the linear Fresnel coefficients for the input visible and IR fields are incorporated in the present definition of χ in eq 1, which is based on the external fields in the vacuum. Equations 1 and 2 do not take account of higher-order polarization terms originating from the bulk.

The term $\chi(\omega_{SFG},\omega_{vis},\omega_{IR})$ depends on the three frequencies and, in particular, on the IR frequency ω_{IR} when the visible and SFG frequencies are off resonance, which is often the case in many applications. We discuss these cases in this paper. In the following, we neglect (the frequency dependence of) the

* To whom correspondence should be addressed. E-mail: amorita@ims.ac.jp.

† Also at Institute for Chemical Research, Kyoto University, Kyoto 611-0011, Japan.

10.1021/jp058155m CCC: $33.50
Published on Web 01/31/2006

nonlinear Fresnel coefficient F_{SFG} in the SFG spectra, that is, $|F_{SFG}\chi|^2 \sim |\chi|^2$.

The variable χ can be decomposed into a resonant term χ^{eyc} and a nonresonant term χ^{NR}, such that $\chi = \chi^R + \chi^{NR}$. The resonant term χ^R governs the vibrational structure of the spectra and can be represented by the time correlation function as[13]

$$\chi^R_{pqr} = \frac{i}{\hbar}(1 - e^{-\hbar\omega_{IR}/k_BT})\int_0^\infty dt\, e^{i\omega_{IR}t}\langle \hat{A}_{pq}(t)\, \hat{M}_r(0)\rangle = \frac{i}{\hbar}\tanh\left(\frac{\hbar\omega_{IR}}{2k_BT}\right)\int_0^\infty dt\, e^{i\omega_{IR}t}\left\langle \frac{1}{2}[\hat{A}_{pq}(t), \hat{M}_r(0)]_+\right\rangle \quad (3)$$

where $\hat{A}(t)$ and $\hat{M}(0)$ are the polarizability and dipole moment operators of the entire system at time t and 0, respectively, in the quantum mechanical Heisenberg representation. The expression $[A, B]_+ = AB + BA$ denotes the anticommutator, and the suffixes p, q, r ($= x-z$) denote the tensor components in space-fixed coordinates. Note that the prefactor of eq 3 originates from the detailed balance condition.[14]

In practical calculations, this quantum mechanical expression of χ^R is replaced by the classical expression χ^R(cl). In the harmonic approximation of vibrational dynamics, the thermal average of the anticommutator corresponds to the classical counterpart with the harmonic correction factor[15] $(\hbar\omega/2k_BT)\coth(\hbar\omega/2k_BT)$. Accordingly χ^R(cl) becomes

$$\chi^R_{pqr}(\mathrm{cl}) = \frac{i}{\hbar}\tanh\left(\frac{\hbar\omega_{IR}}{2k_BT}\right)\frac{\hbar\omega_{IR}}{2k_BT}\coth\left(\frac{\hbar\omega_{IR}}{2k_BT}\right)\int_0^\infty \times dt\, e^{i\omega_{IR}t}\langle A_{pq}(t)\, M_r(0)\rangle_{cl} = \frac{i\omega_{IR}}{2k_BT}\int_0^\infty dt\, e^{i\omega_{IR}t}\langle A_{pq}(t)\, M_r(0)\rangle_{cl} \quad (4)$$

Equation 4 is the classical representation of χ^R, with the quantum correction considered. The following discussion and calculations are based on classical dynamics and the suffix cl will be omitted.

The macroscopic polarizability A and dipole moment M depend on the inter- and intramolecular configuration of the system, and the time development of A and M reflects these molecular motions:

$$A(t) = A(\{\mathbf{r}_{ai}(t)\}), \quad M(t) = M(\{\mathbf{r}_{ai}(t)\}) \quad (5)$$

where $\mathbf{r}_{ai}$ is the position of the ath atom of the ith molecule.

In the computation of eq 4 by a classical molecular dynamics simulation, the force field model has to include intramolecular vibration. To account for $A(t)$ and $M(t)$ in eq 5, the molecular model should represent the dipole moment $p_i^0(\mathbf{r}_{ai})$ and polarizability $\alpha_i^0(\mathbf{r}_{ai})$ of each isolated molecule. The polarizability A and dipole moment M at a given instantaneous configuration are represented as

$$A = \sum_i \alpha_i f(i), \quad M = \sum_i p_i = \sum_i (p_i^0 + \alpha_i E_i) \quad (6)$$

where $f(i)$ is the local field correction factor for the ith molecule, as described in detail in ref 8, and E_i is the electric field acting on the ith molecule by the intermolecular electrostatic interaction. Note that α_i and p_i in eq 6 are the polarizability and the dipole moment of the ith molecule in the condensed phase and, thus, are affected by the perturbation of the surrounding environment. In the calculation for the water surface, $\alpha_i \approx \alpha_i^0$ is assumed in eq 6, though the effect of perturbation on the polarizability may not be negligible in a more rigorous sense.

The nonresonant term χ^{NR} is an important component in the spectral shape and it is desirable to calculate its contribution in a comprehensive spectral analysis. The variable χ^{NR} is of purely electronic origin and is nearly insensitive to the vibrational frequency. Hence, it can be essentially represented as a sum of the electronic hyperpolarizabilities of the constituent molecules, including the local field correction:

$$\chi^{NR}_{pqr} = \left\langle \frac{1}{2}\sum_i \sum_{q'r'}^{x-z} \frac{1}{2}\beta^{el}_{pq'r'}(i)\, f_{q'q}(i)\, f_{r'r}(i)\right\rangle \quad (7)$$

where the suffixes, p, q, r, q', and r', are based on the space-fixed coordinates. The term $\beta^{el}(i)$ is the electronic static hyperpolarizability of the ith molecule, which can be readily calculated by a quantum chemistry calculation suite. Equation 7 has two local field correction factors f acting on the second and third suffixes, q and r. They correspond to the input visible and IR fields, respectively, according to the present definition of χ in eq 1.

Equation 7 has two factors of $^1/_2$. The first is due to the fact that the electronic hyperpolarizability β^{el} is divided by the symmetry number 2, originating from the exchange of suffixes q' and r'.[8] The second factor of $^1/_2$ is derived from the splitting of the static hyperpolarizability into resonant and nonresonant terms.[11]

3. Computation

The present computation of the SFG spectrum of the surface of water is a revision of our previous calculation in ref 8. Here, we describe only the revised points.

The force field of a water molecule is a flexible extension of the SPC water model,[16] with the parameters optimized by Martí et al.[17] to the intramolecular vibrational IR bands of liquid water and D-substituted analogues.

The geometry of liquid water considered here is a slab with two-dimensional periodic boundary conditions. The periodic length L along the two lateral directions, the x and y axes, is 19.7 Å, and one cell contains $N = 256$ water molecules. The thickness of the slab along the vertical (z) axis is accordingly ~20 Å. The number of molecules considered is smaller than that in our previous works[6,8] to allow large statistical sampling calculations. We found that the system size is not critical to the SFG spectrum of neat water, as the signal originates from a monolayer scale at the surface.[6] The temperature was set to $T = 25$ °C in the microcanonical ensemble. The average density profile of the water slab along the z axis is displayed in Figure 1.

As shown in Figure 1, the slab of water has two surfaces, for $z > 0$ and $z < 0$, where $z = 0$ is the center of the slab, and thus, the surface properties are defined for each surface. Accordingly, A, M, and χ^{NR} in eqs 6 and 7 were defined for each half region of $z > 0$ or $z < 0$ and their statistics were treated separately for the two sides, with the quantities in the $z < 0$ region defined on the revised z axis.

This treatment of the statistics could cause practical problems when a molecule moves across the boundary $z = 0$. In that case, the number of molecules in each half region may change discontinuously, which will cause artificial noise in the time correlation function.[9] To prevent the discontinuity, Perry et al.[18] employed an artificial restraining potential at the boundary. In the present work, a smoothing factor

$$g(z_i) = \tanh(|z_i|/w) \quad (8)$$

was applied on the ith molecule for the summations in eqs 6 and 7, where z_i is the z center-of-mass coordinate of the ith

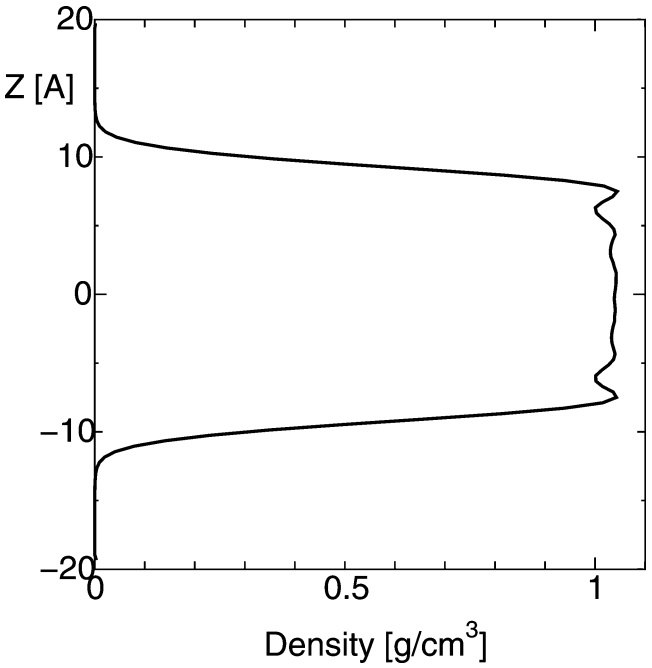

Figure 1. Density profile of the water slab along the vertical direction.

molecule and a width of $w = 1.0$ Bohr (~0.53 Å) was assumed. This treatment effectively alleviates the discontinuity at $z = 0$ without modifying the dynamics near the interface. In connection to this problem, the time correlation function $\langle A(t)M\rangle$ should be valid for a relatively short time within the diffusive temporal scale τ_D, which is typically given as

$$\tau_D \sim (2w)^2/D = 4.9 \text{ ps} \tag{9}$$

where $2w$ is the width of the boundary and D is the diffusion coefficient of a water molecule, $D = 2.3 \times 10^{-9}$ m^2/s at $T =$ 25 °C. To restrict the correlation within this time scale, the calculated time correlation function $\langle A(t)M\rangle$ was damped with a time constant τ_D by a factor e^{-t/τ_D}. This damping factor imposes an intrinsic limitation on the frequency resolution, though this time scale is much longer than that of the intramolecular vibration period by an order of magnitude.

The nonresonant part of the nonlinear susceptibility χ^{NR} is constructed from the electronic molecular hyperpolarizability as described by eq 7, where the electronic hyperpolarizability of the ith molecule $\beta^{el}_{pqr}(i)$ in the space-fixed coordinates was derived from the molecular hyperpolarizability $\beta^{el,mol}$ and the direction cosine matrix $D(i)$ as

$$\beta^{el}_{pqr}(i) = \sum_{p'q'r'}^{x-z} \beta^{el,mol}_{p'q'r'} D_{p'p}(i)\, D_{q'q}(i)\, D_{r'r}(i) \tag{10}$$

In eq 10, $\beta^{el,mol}$ is calculated quantum chemically[19] for an isolated molecule of the equilibrium conformation in molecule-fixed coordinates, while $D(i)$ is determined instantaneously for each molecule. However, our calculations showed that straightforward application of eq 7 does not necessarily provide an optimum nonresonant amplitude relative to the resonant amplitude. In the case of water, the calculated amplitude by eq 7 was exceedingly smaller than the optimum value. Therefore, in this work, we assumed a nonresonant amplitude that best described the experimental spectral shape. For the water surface, the relative magnitude was compared to the available experimental results.[20] An accurate calculation of χ^{NR} requires further details in the molecular model, which will be the subject of

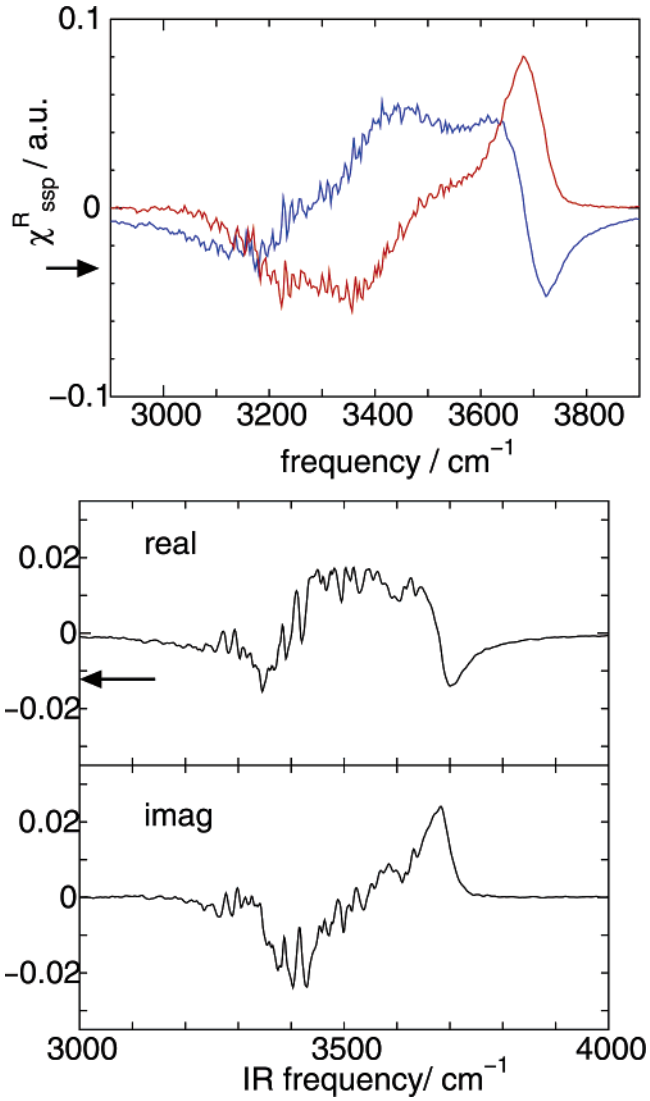

Figure 2. Upper panel: real (blue) and imaginary (red) parts of the resonant nonlinear susceptibility χ^R_{ssp} of the water surface as a function of the infrared frequency. The arrow indicates the assumed nonresonant amplitude. Lower panel: previous calculation of χ^R_{ssp}. The upper and lower plots show the real and imaginary parts, respectively, reproduced with permission from Figure 7c of ref 8. Copyright 2002 American Chemical Society.

future studies. We think that the most important missing factor in eqs 7 and 10 is the effect of perturbation on the molecular hyperpolarizability in the condensed phase, which could be quite substantial.[21,22]

Regarding the computational cost, the most time-consuming part of the computation is the calculation of the local field correction factors.[8] This part includes finding the solutions of linear equations of $3N$-dimensions at each time step. Another problem related to the computational cost is the slow convergence of $\langle A(t)M\rangle$ in the statistical sampling. This becomes particularly problematic when the bulk region(s) have a substantial vibrational density of state in the frequency range overlapping with the interface SFG spectra. Although isotropic bulk in principle produces no nonlinear susceptibility, cancellation of the background bulk noise actually requires a large amount of statistical sampling.

To deal with this problem, statistical sampling calculations were performed by a parallel environment using 256 CPUs (HITACHI HA8000). Each processing unit generated a different trajectory of 570 000 steps with a time step of 0.611 fs. Each

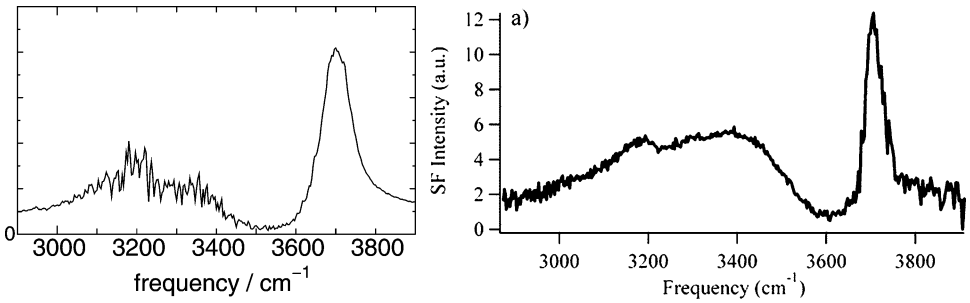

Figure 3. Upper panel: calculated SFG spectrum of the water surface for the *ssp* configuration with the visible wavelength (800 nm) fixed. Lower panel: experimental SFG spectrum, reproduced with permission from ref 20. Copyright 2003 American Chemical Society.

configuration of the water slab corresponded to two surface samples at $z > 0$ and $z < 0$. The time correlation function was calculated along two equivalent directions, $\langle A(t)M\rangle$ and $\langle AM(t)\rangle$, which provided independent sampling in classical dynamics. In addition, computation of the *ssp* (*sps*) signal was performed using both the *xxz* and *yyz* (*xzx* and *yzy*) components of the nonlinear susceptibility χ. To summarize, the total sampling statistics amounts to 256 × 570 000 × 0.611 fs × 2 × 2 × 2 ≈ 713 ns. This sampling corresponds to ∼37 times that of our previous calculation.[8]

4 Results and Discussion

Density Profile. Figure 1 displays the calculated density profile along the *z* axis normal to the surfaces. This interfacial density profile is well-described by a hyperbolic tangent function:

$$\rho(z) = a[1.0 - \tanh(b(|z| - c))] \qquad (11)$$

where $a = 0.518$ g/cm^3, $b = 0.847$ Å^{-1}, and $c = 9.48$ Å. Accordingly, the bulk density is $2a = 1.03$ g/cm^3 and the 10−90 interface thickness t is 2.59 Å. The density profile of Figure 1 also exhibits a small but apparent oscillation near the interface,[23] not represented by the hyperbolic tangent form of eq 11. We also calculated the density profile using $N = 1024$ for comparison, resulting in a 10−90 thickness of 3.14 Å. It appears that the smaller cell with $N = 256$ yielded a somewhat narrower surface.[24] This 10−90 thickness is comparable with our previous result calculated using Ferguson's model,[25] 3.18 Å at 302 K.[8] Both the flexible SPC models of Martí[17] and Ferguson[25] produce a slightly more compact surface than the SPC/E model, yielding $t = 3.32$ Å (with $N = 526$) or 3.57 Å ($N = 1056$) at $T = 298$ K.[24]

***ssp* Susceptibility.** The *ssp* component of the vibrationally resonant nonlinear susceptibility χ^R_{ssp} of liquid water is shown in Figure 2. The calculated result of χ^R_{ssp} is qualitatively comparable to our previous calculation,[8] which is also displayed in Figure 2 for comparison. The two calculation results both show that the imaginary part of χ^R_{ssp} changes sign in the peak frequency region at ∼3700 cm^{-1} and in the 3000−3500 cm^{-1} region. The former band is assigned to the dangling O−H stretching vibration at the surface.[5,26]

The present result of χ^R_{ssp} shows two improvements over the previous result. First, the new band shape has an apparently reduced noise level, particularly in the 3200−3600 cm^{-1} region, allowing a more detailed investigation of the spectral structure and a greater accuracy of the molecular model. The better signal-to-noise ratio results from larger sampling statistics and the boundary treatment described in section 3. Second, the resonant feature at ∼3200 cm^{-1}, corresponding to a relatively large red shift of the O−H stretching vibration, is significantly enhanced. This enhanced amplitude is clearly seen in the imaginary part of χ^R_{ssp}, shown by the red line in Figure 2. This difference can be attributed to the intramolecular force field of the water molecule. The present calculation leads to a spectrum more consistent with experiments in this spectral region, as discussed below.

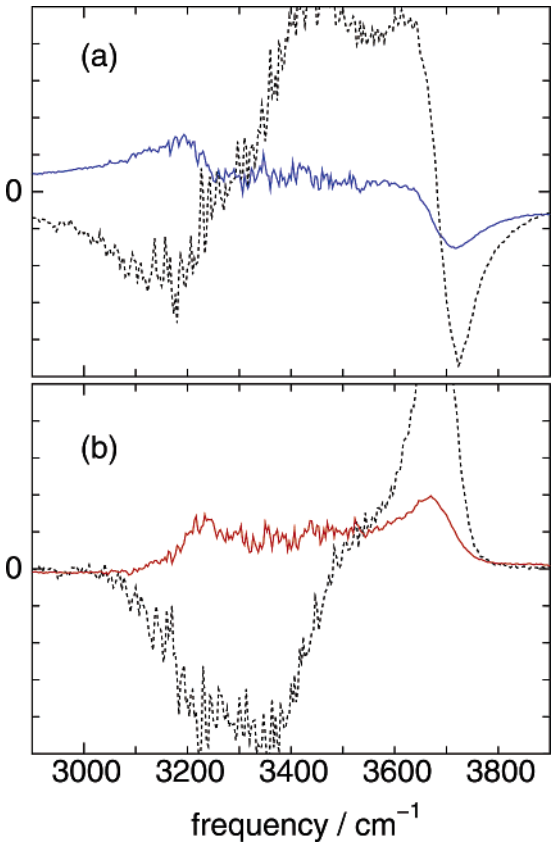

Figure 4. (a) Real and (b) imaginary parts of the vibrationally resonant *sps* susceptibility χ^R_{sps} of water. The dotted lines are the corresponding *ssp* components χ^R_{ssp} for comparison.

In the present work, a nonresonant amplitude χ^{NR} of the water surface was assumed so as to best describe the experimental spectral shape, indicated by the arrow in Figure 2. The relative magnitude of the amplitude is consistent with the experimental value derived from H−D substitution.[20]

Calculated *ssp* Spectrum. The calculated SFG spectrum is displayed in Figure 3. This spectrum is compared with a recent experimental spectrum by Raymond and Richmond,[20] shown in the right panel of Figure 3. The comparison indicates a satisfactory agreement.[27] Other recent experiments by Wei and Shen[10] and by Liu et al.[28] report qualitatively consistent *ssp* spectra for the water−vapor interface.

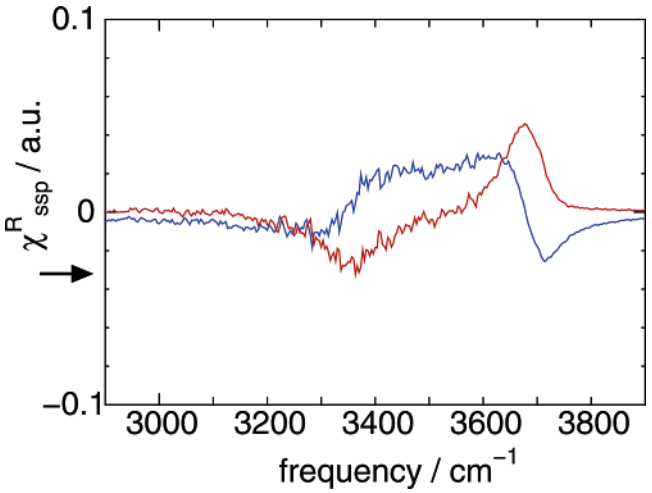

Figure 5. Real (blue) and imaginary (red) parts of the resonant nonlinear susceptibility χ^R_{ssp} of HDO water surface. The arrow indicates the assumed nonresonant background.

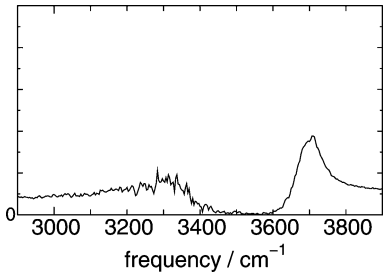

Figure 6. Calculated *ssp* spectrum of HDO water surface.

While the molecular dynamics calculation of SFG spectroscopy is suitable for determining the phase information of the nonlinear susceptibility, recently, Ostroverkhov et al.[29] experimentally measured the phase of the *ssp* susceptibility at water−quartz interfaces. Interestingly, the reported phase behavior at the water−quartz interfaces is quite different from that at the water−vapor interface, implying that the interface water structure is quite sensitive to the substrate.

***sps* Component.** Figure 4 displays the *sps* component of the resonant susceptibility, χ^R_{sps}. The present computation reveals that the *sps* component is quite different from the *ssp* component, which is also shown in Figure 4 by the dotted lines. The *sps* amplitude is much smaller than the *ssp* amplitude over the frequency range of the O−H stretching vibration, consistent with the findings of previous experiments.[10,26] Also, the sign of the imaginary part of *sps* does not change between the 3700 cm^{-1} (dangling O−H stretching) region and the 3000−3500 cm^{-1} (hydrogen-bonded O−H stretching) region. The constant sign of the *sps* component is quite contrary to the imaginary part of *ssp*.

The calculated *sps* amplitude predicts a small resonant peak at ∼3700 cm^{-1}, whereas another experimentally observed small resonant feature at ∼3600 cm^{-1} (ref 10) is not apparent in Figure 4. The reason for this discrepancy is not clear at present. The derivation of the *sps* spectrum is more difficult than that of the *ssp* spectrum, due to a lack of information on the nonresonant component and the bulk contribution. While the present computation does not take account of the bulk contribution, presumably, it is not negligible in the *sps* component.[30] A more comprehensive analysis of the *sps* spectrum is needed.

HDO Case. The isotope substitution technique is a powerful tool in analyzing vibrational spectra. Richmond et al. employed H−D isotopic dilution in vibrational SFG spectroscopy of water and aqueous solutions[20,31,32] and succeeded in decomposing the nonresonant background and analyzing resonant features in the experimental spectra. Motivated by their success, we calculated the *ssp* spectrum of HDO water, where the force field and MD conditions are the same as those of H_2O water, except for the hydrogen mass. Although experimental samples are necessarily a mixture of HDO, H_2O, and D_2O due to facile H−D exchange, pure HDO water should be considered as an ideal reference where all the intramolecular coupling of the O−H/D stretching is effectively removed.

The resonant susceptibility and spectrum for HDO water are given in Figures 5 and 6, respectively. In deriving the HDO spectrum of Figure 6, the amplitude of the nonresonant background was assumed to be same as for H_2O. In comparing χ^R_{ssp} of H_2O in Figure 2 to that of HDO in Figure 5, it can be seen that the amplitude of the ∼3700 cm^{-1} peak is nearly one-half in the HDO case, which is understandable from the relative number density of the O−H dangling bonds of H_2O water and HDO water. While the overall shape of the HDO susceptibility amplitude χ^R_{ssp} is similar to that of H_2O, there is little resonance in the low-frequency region at ∼3200 cm^{-1} for HDO. This can be attributed to the lack of a symmetric stretching component in the HDO case.

5. Concluding Remarks

Theoretical computation of the sum frequency generation spectroscopy via molecular dynamics simulation is potentially quite powerful in helping exploit molecular information from SFG experiments. We are currently developing theoretical and computational methods, as described in this paper. The improved computation of the SFG spectra of water is demonstrated and reproduces the experimental spectra with nearly comparable accuracy. We think that this is an important step toward practical applications of SFG computation.

Some issues remain to be addressed in the computation of SFG spectroscopy. Calculation of the nonresonant susceptibility should be significantly improved by considering solvent perturbation on electronic molecular hyperpolarizability. For the comprehensive analysis of observed SFG spectra, evaluation of the bulk contribution is necessary. To expand the application to systems other than water, a general and accurate molecular model for SFG calculation is required. We are currently working on the above issues.

Acknowledgment. The author thanks Prof. Casey Hynes and the anonymous reviewer for their useful comments. This work was supported by a Grant-in-Aid (No. 15550012) and the National Research Grid Initiative (NAREGI) of the Ministry of Education, Japan. Calculations were performed at the Research Center for Computational Science, Okazaki, Japan.

References and Notes

(1) Buck, M.; Himmelhaus, M. *J. Vac. Sci. Technol. A* **2001**, *19*, 2717−2736.
(2) Bain, C. D. *J. Chem. Soc., Faraday Trans.* **1995**, *91*, 1281−1296.
(3) Miranda, P. B.; Shen, Y. R. *J. Phys. Chem. B* **1999**, *103*, 3292−3307.
(4) Shultz, M. J.; Schnitzer, C.; Simonelli, D.; Baldelli, S. *Int. Rev. Phys. Chem.* **2000**, *19*, 123−153.
(5) Richmond, G. L. *Chem. Rev.* **2002**, *102*, 2693−2724.
(6) Morita, A.; Hynes, J. T. *Chem. Phys.* **2000**, *258*, 371−390.
(7) Yeh, Y. L.; Zhang, C.; Held, H.; Mebel, A. M.; Wei, X.; Lin, S. H.; Shen, Y. R. *J. Chem. Phys.* **2001**, *114*, 1837−1843.
(8) Morita, A.; Hynes, J. T. *J. Phys. Chem. B* **2002**, *106*, 673−685.
(9) Perry, A.; Ahlborn, H.; Space, B.; Moore, P. B. *J. Chem. Phys.* **2003**, *118*, 8411−8419.
(10) Wei, X.; Shen, Y. R. *Phys. Rev. Lett.* **2001**, *86*, 4799−4802.

(11) Morita, A. *Chem. Phys. Lett.* **2004**, *398*, 361−366.
(12) Shen, Y. R. In *Surface Spectroscopy by Nonlinear Optics*; Hansch, T., Inguscio, M., Eds.; North-Holland: Amsterdam, 1994; Vol. CXX.
(13) Pouthier, V.; Hoang, P. N. M.; Girardet, C. *J. Chem. Phys.* **1999**, *110*, 6963−6976.
(14) Mukamel, S. *Nonlinear Optical Spectroscopy*; Oxford University Press: New York, 1995.
(15) Bader, J. S.; Berne, B. J. *J. Chem. Phys.* **1994**, *100*, 8359−8366.
(16) Berendsen, H. J. C.; Postma, J. P. M.; van Gunsteren, M. F.; Hermans, J. Interaction Models for Water in Relation to Protein Hydration. In *Intermolecular Forces*; Pullman, B., Ed.; Reidel: Dordrecht, The Netherlands, 1981.
(17) Martí, J.; Padró, J. A.; Guàrdia, E. *J. Mol. Liq.* **1994**, *62*, 17−31.
(18) Perry, A.; Neipert, C.; Ridley, C.; Space, B. *Phys. Rev. E* **2005**, *71*, 050601.
(19) Maroulis, G. *Chem. Phys. Lett.* **1998**, *289*, 403−411.
(20) Raymond, E. A.; Tarbuck, T. L.; Brown, M. G.; Richmond, G. L. *J. Phys. Chem. B* **2003**, *107*, 546−556.
(21) Bishop, D. M. *Int. Rev. Phys. Chem.* **1994**, *13*, 21−39.
(22) Bella, S. D.; Marks, T. J.; Ratner, M. A. *J. Am. Chem. Soc.* **1994**, *116*, 4440−4445.
(23) Sokhan, V. P.; Tildesley, D. J. *Mol. Phys.* **1997**, *92*, 625−640.
(24) Taylor, R. S.; Dang, L. X.; Garrett, B. C. *J. Phys. Chem.* **1996**, *100*, 11720−11725.
(25) Ferguson, D. M. *J. Comput. Chem.* **1995**, *15*, 501−511.
(26) Du, Q.; Superfine, R.; Freysz, E.; Shen, Y. R. *Phys. Rev. Lett.* **1993**, *70*, 2313−2316.
(27) Reference 20 shows two spectra, with and without calibration by the infrared refractive index. The present simulation should be compared with the experimental spectrum without the calibration, as discussed in section 2.
(28) Liu, D.; Ma, G.; Levering, L. M.; Allen, H. C. *J. Phys. Chem. B* **2004**, *108*, 2252−2260.
(29) Ostroverkhov, V.; Waychunas, G. A.; Shen, Y. R. *Phys. Rev. Lett.* **2005**, *94*, 046102.
(30) Held, H.; Lvovsky, A. I.; Wei, X.; Shen, Y. R. *Phys. Rev. B* **2002**, *66*, 205110.
(31) Raymond, E. A.; Tarbuck, T. L.; Richmond, G. L. *J. Phys. Chem. B* **2002**, *106*, 2817−2820.
(32) Raymond, E. A.; Richmond, G. L. *J. Phys. Chem. B* **2004**, *108*, 5051−5059.